Model for the Attosecond Resonant Photoemission of Copper Dichloride: Evidence for High-Order Fano Resonances and a Time-Domain Core-Hole Clock

J. D. Lee

Department of Emerging Materials Science, DGIST, Daegu 711-873, Korea

(Received 30 October 2012; published 9 July 2013)

We present a model of the attosecond resonant dynamics of valence electron photoemission and MMM Auger electron emission in copper dichloride. At $\tau_h \gg 1/\omega_{\mathrm{IR}}$ (where τ_h is the core-hole relaxation time and ω_{IR} is the energy of the infrared probe field), high-order Fano sideband resonances on both sides of the original (zeroth-order) resonance are found in the energy domain on the time scale of τ_h. This is confirmed by a coherent π rotation of the relative phase between the photoelectron and Auger electron at each resonance, due to the subfemtosecond quantum correlation. We also find a core-hole clock, the asymmetry factor q of the first-order Fano sideband resonance, which can directly trace the core-hole relaxation in the time domain.

DOI: 10.1103/PhysRevLett.111.027401 PACS numbers: 78.47.J−, 42.50.Hz, 78.20.Bh, 79.60.−i

An extreme ultraviolet (XUV) light source with attosecond (as) (1 as $= 10^{-18}$ s) pulse duration allows new time-domain insight at the time scale of 10–100 as well as into the electron dynamics occurring within atoms, molecules, and solids [1–5]. Photoemission may accompany the inner-shell vacancy, which rapidly relaxes owing to its excess internal energy in $\lesssim$1 fs (1 fs $= 10^{-15}$ s) with a concomitant emission of another electron, the Auger electron emission [1,6,7]. A sequence of events, originally relating to the electron Coulomb correlation, is usually beyond the reach of femtosecond optical measurement. This provides motivation for the attosecond time-domain exploration of a solid with strongly correlated electrons [8].

One of the most dramatic phenomena of quantum interference in solid state physics may be asymmetric Fano resonance [9]. This occurs when two quantum mechanically coupled excitation paths to a quasidiscrete configuration and to a continuum manifold interfere with each other. Resonant photoemission, first discovered in atomic He, Ne, and Ar [10] and out of solid systems in nickel metal [11], gives the Fano resonance leading to a resonant enhancement of a particular final state. It stems from interference between the direct photoemission of a valence electron and the autoionization of a photoexcited quasidiscrete configuration (i.e., the Auger process).

The ground state of $CuCl_2$ is written as $3d^9$ [see the inset of Fig. 1(a)] with a filled ligand shell L; i.e., $3d^9$ and L refer to Cu^{2+} and Cl^- for $CuCl_2$, respectively. Photoemission of the valence band of $CuCl_2$ shows the presence of the $3d^8$ satellite as well as the main lines of $3d^9L^{-1}$ or $3d^{10}L^{-2}$ [where $L^{-1(2)}$ denotes a ligand with one (two) hole(s)] [12,13]. The $3d^8$ satellite incorporates the strong Coulomb correlation in the final state and the breakdown of a single-particle model, for which we note $3d^9 + \omega_{\mathrm{XUV}} \rightarrow 3d^8 + e^-$ [$\varepsilon_{\mathbf{k}} = \omega_{\mathrm{XUV}} - E_{3d^8}$; $\varepsilon_{\mathbf{k}}$ is the kinetic energy of e^- (a continuum electron), ω_{XUV} is the energy of the XUV pump field, and E_{3d^8} is the energy of the $3d^8$ satellite]. Meanwhile, the excitation $3p \rightarrow 3d$ in Cu^{2+} is followed by the Auger decay and autoionization, $3p^63d^9 + \omega_{\mathrm{XUV}} \rightarrow 3p^53d^{10} \rightarrow 3p^63d^8 + e^-$ ($\varepsilon_{\mathbf{k}} = \varepsilon_p - E_{3d^8}$; ε_p is the energy of the Cu $3p$ hole), i.e., a super Coster-Kronig process, which corresponds to the MMM Auger emission. At $\omega_{\mathrm{XUV}} = \varepsilon_p$, the same final state $|\mathbf{k}\rangle|3d^8\rangle$ with the same kinetic energy $\varepsilon_{\mathbf{k}} = \varepsilon_p - E_{3d^8}$ is reached by the two emission processes. The two processes then overlap coherently and provide Fano resonance leading to a resonant enhancement in the $3d^8$ satellite [13,14]. This is the original stationary version of the resonant photoemission of $CuCl_2$.

In this Letter, we investigate the time-resolved resonant dynamics of valence electron photoemission and MMM Auger electron emission in $CuCl_2$ in the subfemtosecond time span. For slow core-hole relaxation [i.e., $\tau_h \gg 1/\omega_{\mathrm{IR}}$ (τ_h: core-hole relaxation time and ω_{IR}: energy of infrared (IR) probe field)], we find high-order Fano sideband resonances around the well-known original (zeroth-order) resonance in the energy domain up to the time of a few τ_h's. This is confirmed by a coherent π rotation of the relative phase between the photoelectron and Auger electron as the energy traverses each resonance, which is a clear manifestation of the subfemtosecond quantum correlation between two-hole states of the system. Incidentally, the (zeroth-order) Fano main resonance in attosecond autoionization of atomic Ar and He was recently demonstrated [15,16], but the high-order Fano sideband resonance was not indicated because the phase investigation for high-order sideband resonances was lacking. In contrast, new importance is explored in the high-order Fano sideband resonance. We find that the asymmetry factor q of the first-order Fano sideband resonance can directly trace the core-hole relaxation dynamics. This is the first finding of a true core-hole clock that works in the time domain.

A strongly correlated electron system including d electrons (or holes) can often be simplified by employing the molecular orbital approach owing to the localized nature of the electrons [14]. The ground state $|0\rangle$ of $CuCl_2$, the $3d^9$ configuration with a single hole, is obtained from $\mathcal{H}(\tau = -\infty) = \varepsilon_{d_1} d_1^\dagger d_1 + \varepsilon_{L_1} l_1^\dagger l_1 + t_1(d_1^\dagger l_1 + l_1^\dagger d_1)$: $|0\rangle = \cos\theta|d_1\rangle - \sin\theta|l_1\rangle$ with $\tan 2\theta = 2t_1/(\varepsilon_{L_1} - \varepsilon_{d_1})$, where ε_{d_1} and ε_{L_1} are energy levels of the Cu $3d$ hole ($d_1^\dagger$ or d_1 is the $3d$ hole operator), and the ligand hole ($l_1^\dagger$ or l_1 is the ligand hole operator). To describe the valence electron photoemission, we propose $\mathcal{H}_0$ modeling $CuCl_2$ with two holes,

$$\mathcal{H}_0 = \varepsilon_{d_1} d_1^\dagger d_1 + \varepsilon_{d_2} d_2^\dagger d_2 + \varepsilon_{L_1} l_1^\dagger l_1 + \varepsilon_{L_2} l_2^\dagger l_2 + t_1(d_1^\dagger l_1 + l_1^\dagger d_1) + t_2(d_2^\dagger l_2 + l_2^\dagger d_2) + U n_{d_1} n_{d_2}, \quad (1)$$

where the index "2" indicates the symmetry of the second hole (created by the photoemission) [17], and U is the Coulomb repulsion between two Cu $3d$ holes. For necessary parameters, we take $\varepsilon_{d_1} = \varepsilon_{d_2} = 0$, $\varepsilon_{L_1} = \varepsilon_{L_2} = 2.72$ eV, $t_1 = t_2 = 2$ eV for all valence states, and $U = 9.5$ eV. Small energy differences between $3d$ holes at d_1 and d_2 orbitals, or between ligand holes at l_1 and l_2 orbitals, are neglected for the sake of simplicity. Diagonalizing $\mathcal{H}_0$ with a basis set $\{|d_1\rangle|d_2\rangle, |d_1\rangle|l_2\rangle, |l_1\rangle|d_2\rangle, |l_1\rangle|l_2\rangle\}$, four final states after photoemission are obtained. Among those, the two energetically lowest states have a configuration of $3d^9L^{-1}$, and the other two have a configuration of $3d^{10}L^{-2}$ and $3d^8$. In fact, $|3d^8\rangle$ is the highest excited state owing to a large Coulomb repulsion U. Its binding energy E_{3d^8} is obtained as 10.75 eV from the adopted parameters, which agrees well with experimental results [13].

$\mathcal{H}_1(\tau)$ comprises the photoexcitations due to the XUV pulse, the Auger interaction, and the probing of the continuum electron by the IR pulse,

$$\mathcal{H}_1(\tau) = \sum_{\mathbf{k}} \Delta_{d_2\mathbf{k}}(c_{\mathbf{k}}^\dagger d_2^\dagger + d_2 c_{\mathbf{k}}) A_{\mathrm{XUV}}(\tau) + \varepsilon_p p^\dagger p + \Delta_{d_1 p}(p^\dagger d_1 + d_1^\dagger p) A_{\mathrm{XUV}}(\tau) + M\sum_{\mathbf{k}}(c_{\mathbf{k}}^\dagger p d_1^\dagger d_2^\dagger + d_2 d_1 p^\dagger c_{\mathbf{k}}) + \sum_{\mathbf{k}}[\varepsilon_{\mathbf{k}} - \mathbf{k}\cdot\mathbf{A}_{\mathrm{IR}}(\tau - \tau_{\mathrm{IR\text{-}XUV}})] c_{\mathbf{k}}^\dagger c_{\mathbf{k}}, \quad (2)$$

where $c_{\mathbf{k}}^\dagger$ or $c_{\mathbf{k}}$ is the operator of the continuum electron with kinetic energy $\varepsilon_{\mathbf{k}} = \mathbf{k}^2/2$, and $p^\dagger$ or p is the operator of the Cu $3p$ hole with an energy level of ε_p (=72 eV). M parametrizes the Auger matrix element given by the Coulomb potential. $\mathbf{A}_{\mathrm{XUV}}(\tau)$ is the photoexciting XUV pulse given by $\mathbf{A}_{\mathrm{XUV}}(\tau) = A_{\mathrm{XUV}} \exp[-0.036\tau^2] \times \cos(\omega_{\mathrm{XUV}}\tau)\hat{\mathbf{e}}_{\mathrm{XUV}}$, and $\mathbf{A}_{\mathrm{IR}}(\tau)$ is the probing IR pulse given by $\mathbf{A}_{\mathrm{IR}}(\tau) = A_{\mathrm{IR}} \exp[-4.37 \times 10^{-5}\tau^2] \cos(\omega_{\mathrm{IR}}\tau)\hat{\mathbf{e}}_{\mathrm{IR}}$. A_{XUV} and A_{IR} are field strengths of the two pulses. $\bar{\tau}_{\mathrm{XUV}}$ and $\bar{\tau}_{\mathrm{IR}}$ are the half widths at half maximum of the XUV and IR pulses; i.e., $\bar{\tau}_{\mathrm{XUV}} = 4.4$ a.u. $= 105$ as and $\bar{\tau}_{\mathrm{IR}} = 125.9$ a.u. $= 3$ fs. $\tau_{\mathrm{IR\text{-}XUV}}$ is a controllable relative delay of the IR pulse from the XUV pulse. $\Delta_{d_2\mathbf{k}}$ or $\Delta_{d_1 p}$ would be $\langle\mathbf{k}|\Delta|d_2\rangle$ or $\langle p|\Delta|d_1\rangle$ of the dipole operator Δ ($= \mathbf{r}\cdot\hat{\mathbf{e}}_{\mathrm{XUV}}$). Noting that the $\mathbf{k}$ dependence of $\Delta_{d_2\mathbf{k}}$ is usually weak, we take $\Delta_{d_2\mathbf{k}}$ just as a constant.

Under the total Hamiltonian of $\mathcal{H}(\tau)$ [$= \mathcal{H}_0 + \mathcal{H}_1(\tau)$], by solving the time-dependent Schrödinger equation with $A_{\mathrm{XUV}} \to 0$, we can treat the relevant electron (or hole) dynamics in an exact fashion. The quantum mechanical wave function $|\Psi(\tau)\rangle$ that describes the total system at time τ is

$$|\Psi(\tau)\rangle = C_{d_1}(\tau)|d_1\rangle + C_{l_1}(\tau)|l_1\rangle + C_p(\tau)|p\rangle + \sum_{\mathbf{k}}[C_{\mathbf{k}}^{d_1 d_2}(\tau)|\mathbf{k}\rangle|d_1\rangle|d_2\rangle + C_{\mathbf{k}}^{d_1 l_2}(\tau)|\mathbf{k}\rangle|d_1\rangle|l_2\rangle + C_{\mathbf{k}}^{l_1 d_2}(\tau)|\mathbf{k}\rangle|l_1\rangle|d_2\rangle + C_{\mathbf{k}}^{l_1 l_2}(\tau)|\mathbf{k}\rangle|l_1\rangle|l_2\rangle]. \quad (3)$$

Dynamics start by turning on the XUV pulse from the initial ground state $|\Psi(\tau_0)\rangle = |0\rangle$ with $\tau_0 \ll -\bar{\tau}_{\mathrm{XUV}}$. $\tau_0 = -15$ a.u. is taken. Hereafter, $\omega_{\mathrm{IR}} = 1.65$ eV and $\omega_{\mathrm{XUV}} = \varepsilon_p$ are also adopted, unless mentioned otherwise. Figure 1(a) illustrates the time-dependent creation of continuum electrons through $\partial/\partial\tau \sum_{\mathbf{k}} \mathcal{C}_{\mathbf{k}}(\tau)$ with $\mathcal{C}_{\mathbf{k}}(\tau) = |C_{\mathbf{k}}^{d_1 d_2}(\tau)|^2 + |C_{\mathbf{k}}^{d_1 l_2}(\tau)|^2 + |C_{\mathbf{k}}^{l_1 d_2}(\tau)|^2 + |C_{\mathbf{k}}^{l_1 l_2}(\tau)|^2$ for photoemission or Auger emission. It is found that the emission of the photoelectron is fast following the temporal intensity profile of the XUV pulse, while the Auger electron emission drastically depends on M, which determines the core-hole relaxation. τ_h is scaled by M^{-2} as in Fig. 1(b).

Electron spectrograms probed by the IR field, which could in fact be obtained experimentally, are calculated from $S_{3d^8}(\mathbf{k}, \tau_{\mathrm{IR\text{-}XUV}}) = |\langle\mathbf{k}|\langle 3d^8|\Psi(\tau_{\max})\rangle|^2$ for the final state $|3d^8\rangle$. The value of $\tau_{\max}$ that guarantees temporal convergence strongly depends on M [18], as expected

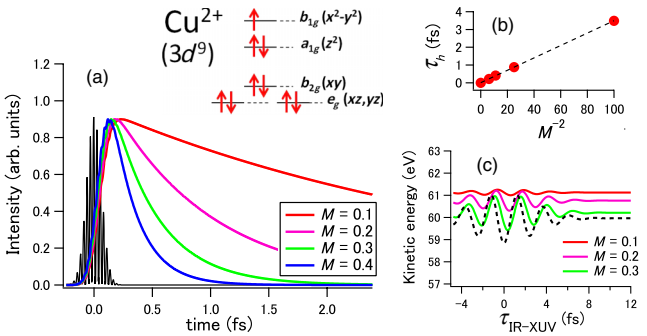

FIG. 1 (color online). (a) Time derivatives of photoelectron (black line) and Auger electron (depending on M) creation; i.e., $(\partial/\partial\tau)\sum_{\mathbf{k}}\mathcal{C}_{\mathbf{k}}(\tau)$. Inset: Energy levels of Cu^{2+} $3d$ electrons, which relate to the local crystal field at the Cu site in a $CuCl_6$ cluster of $CuCl_2$. (b) The relation of τ_h with respect to M. $\tau_h \propto M^{-2}$ is found. (c) Centers of energy of spectrograms of the photoelectron for the $3d^8$ satellite (black dashed line) and Auger electron with respect to a relative delay $\tau_{\mathrm{IR\text{-}XUV}}$. $A_{\mathrm{IR}} = 0.02$ is taken [21]. Units of M and A_{IR} are a.u. (atomic unit).

from Fig 1(a). Moreover, we take $(\varepsilon_{\mathbf{k}})_{\max} = 340$ eV and $N_{\mathbf{k}} = 2400$, which can give sufficient convergence. In Fig. 1(c), the electron emission timing might be compared, but $M = 0.1$ is found rather far from the streaking limit as will be shown later.

Figures 2(a)–2(c) present $S^{\mathrm{AUG}}_{3d^8}(\mathbf{k}, \tau_{\text{IR-XUV}})$ (the Auger electron spectrogram) and $S^{\mathrm{RES}}_{3d^8}(\mathbf{k}, \tau_{\text{IR-XUV}})$ [the total resonant spectrogram of the photoelectron and Auger electron (including interferences between the two)]. In particular, for rather slow core-hole relaxation (e.g., $M = 0.1$), the Auger sidebands appear around the resonance energy in $S^{\mathrm{AUG}}_{3d^8}(\mathbf{k}, \tau_{\text{IR-XUV}})$. Analytically, starting from the Volkov equation under strong fields, $S^{\mathrm{AUG}}_{3d^8}(\mathbf{k}, \tau_{\text{IR-XUV}})$ can be shown to form high-order sidebands at $\varepsilon_k = n\omega_{\text{IR}} + \varepsilon_p - E_{3d^8}$ ($n = \pm 1, \pm 2, \ldots,$) with bandwidth $1/\tau_h$ besides the zeroth-order ($n = 0$) band [19], as seen in the upper panels of Figs. 2(a) and 2(b). That is, $1/\tau_h \ll \omega_{\text{IR}}$ (i.e., slow core-hole relaxation) will be a natural condition in which high-order sidebands appear in a robust way. This was observed in the laser-assisted Auger decay first in Ar [6] and later in Kr [1]. Moreover, high-order sidebands produce resonances with the broadband valence electron photoemission, as explicitly shown in Figs. 2(d)–2(f) [20]. Schematics of the resonance are depicted in Fig. 3(a). Resonance also has characteristic dynamics. The first-order ($n = 1$) sideband resonance near 62.9 eV has a sharp peak at $\tau_{\text{IR-XUV}} = 1.34$ fs [Fig. 2(d)] but a dip at $\tau_{\text{IR-XUV}} = 7.51$ fs [Fig. 2(e)]. This will be illustrated in more detail in Fig. 4.

According to a general solution of the Fano problem, the transition amplitude $\langle\Psi_E|\mathcal{T}|0\rangle$ ($\mathcal{T}$: transition operator) from the ground state $|0\rangle$ to the state $|\Psi_E\rangle$ is $\langle\Psi_E|\mathcal{T}|0\rangle = (1/V_E^*)\langle 1_E|\mathcal{T}|0\rangle \sin\phi_E - \langle E|\mathcal{T}|0\rangle \cos\phi_E$ [9]. $|1\rangle$ is the quasidiscrete state, $|E\rangle$ is the continuum state with energy E, and V_E is the matrix element between $|1\rangle$ and $|E\rangle$. $|1_E\rangle$ and ϕ_E are then given by $|1_E\rangle = |1\rangle + \mathcal{P}\int dE' V_{E'}^*/(E - E')|E'\rangle$ and $\phi_E = -\tan^{-1}[\pi|V_E|^2/(E - E_{\text{RES}})]$. E_{RES} is the resonance energy. The correspondence with our problem becomes obvious by taking $|1\rangle$ as the state of $3p^5 3d^{10}$ and V_E as the Auger matrix element M. Therefore, the first channel of $\langle\Psi_E|\mathcal{T}|0\rangle$ will be the Auger emission, and the second the photoemission.

The most peculiar feature of the Fano resonance should be the sharp phase coherence between two channels due to the interchannel correlation. It is known that the relative phase $\Delta\varphi$ between two competing channels varies swiftly by π as the energy traverses an interval $\sim V_E^2$ ($\sim M^2$ in our case) around the resonance [18]. Figures 3(b) and 3(c) show that such phase correlation is realized not only for the zeroth-order ($n = 0$) resonance but also for the high-order ($n > 0$) sideband resonances in a dramatic fashion, which is evident by a careful comparison of $\Delta\varphi$ and Auger sideband energies given in Fig. 3(e). This is a clear manifestation of the subfemtosecond quantum correlation between two-hole states of the system. Quantum phase

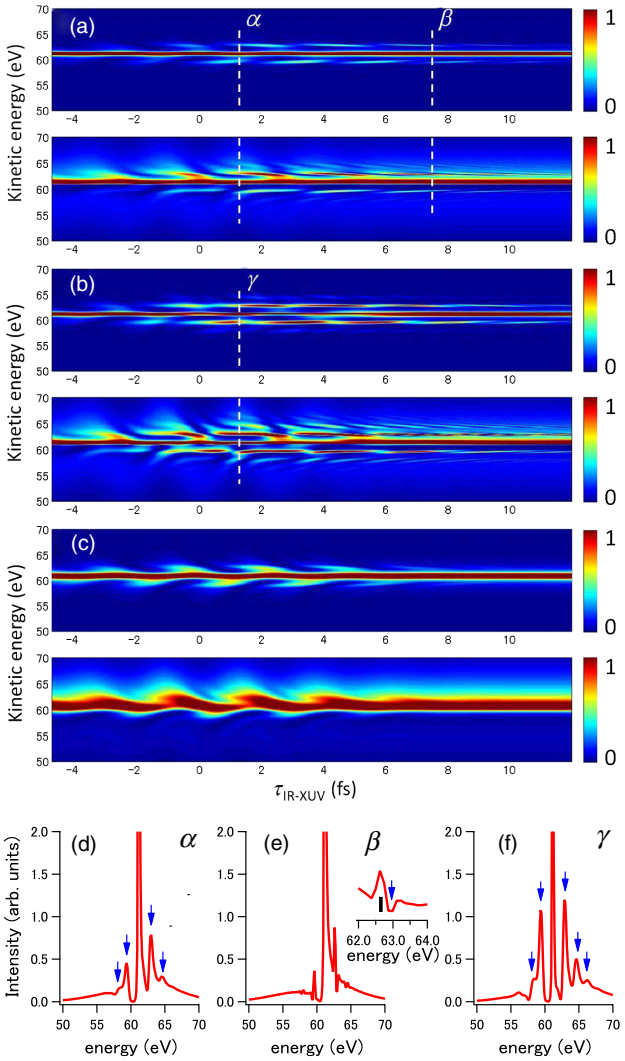

FIG. 2 (color online). Upper panels of (a)–(c): Spectrogram of Auger emission $S^{\mathrm{AUG}}_{3d^8}(\mathbf{k}, \tau_{\text{IR-XUV}})$. Lower panels of (a)–(c): Resonant spectrogram $S^{\mathrm{RES}}_{3d^8}(\mathbf{k}, \tau_{\text{IR-XUV}})$ from a superposition of photoemission and Auger emission. (a) $M = 0.1$ and $A_{\text{IR}} = 0.02$, (b) $M = 0.1$ and $A_{\text{IR}} = 0.04$, and (c) $M = 0.3$ and $A_{\text{IR}} = 0.02$ [21]. (d)–(f) Sliced spectra of $S^{\mathrm{RES}}_{3d^8}(\mathbf{k}, \tau_{\text{IR-XUV}})$ at the positions of α, β, and γ of (a) and (b). Blue arrows indicate high-order sideband resonances. A peak by a black bar in the inset of (e) is an incoherent one.

shifts of $\Delta\varphi$ by π (i.e., red $\rightleftharpoons$ blue) around the high-order sideband resonances confirm that these resonances are in fact the Fano resonances too.

A peak-to-dip change of the first-order ($n = 1$) Fano sideband resonance near 62.9 eV with respect to $\tau_{\text{IR-XUV}}$ is extensively investigated for both $A_{\text{IR}} = 0.02$ and 0.04 in Figs. 4(a) and 4(b). A deeper understanding can be gained using the Fano formula $|\langle\Psi_E|\mathcal{T}|0\rangle|^2 \propto (E - E_{\text{RES}} + q/\tau_h)^2/((E - E_{\text{RES}})^2 + 1/\tau_h^2)$, where the asymmetry factor q is given by the ratio of amplitudes of two competing channels; i.e., $q = \tau_h V_E^* \langle 1_E|\mathcal{T}|0\rangle/\langle E|\mathcal{T}|0\rangle$. Applying the formula to the first-order ($n = 1$) Fano sideband

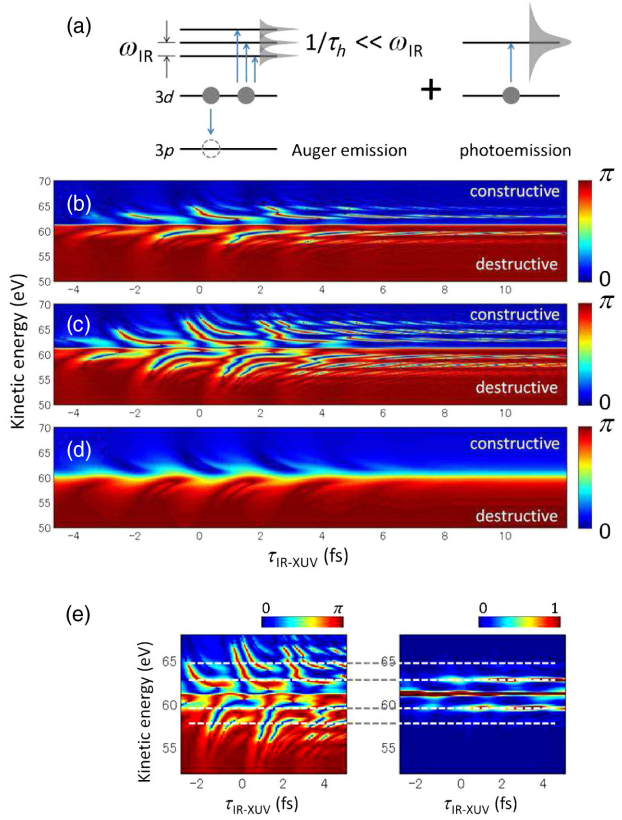

FIG. 3 (color online). (a) Resonance of Auger sidebands and photoemission. (b)–(d) Relative phase $\Delta\varphi$ between the photoelectron (for the $3d^8$ satellite) and Auger electron. (b) $M = 0.1$ and $A_{IR} = 0.02$, (c) $M = 0.1$ and $A_{IR} = 0.04$, and (d) $M = 0.3$ and $A_{IR} = 0.02$. (e) Comparison of $\Delta\varphi$ (left) and Auger sidebands (right) for $M = 0.1$ and $A_{IR} = 0.04$.

resonance yields $q \propto \langle 1_E^{n=1}|\mathcal{T}|0\rangle/\langle E^{n=1}|\mathcal{T}|0\rangle$. Within time-dependent perturbation theory, we further note

$$|1_E^{n=1}\rangle \propto |1_E^{n=0}\rangle \times \int d\tau e^{i\omega_{IR}\tau}\langle 1_E^{n=0}|\mathcal{H}|1_E^{n=1}\rangle,$$

$$\propto |1_E^{n=0}\rangle \times e^{-\tau_{IR\text{-}XUV}/\tau_h} e^{i\omega_{IR}\tau_{IR\text{-}XUV}} A_{IR}(\omega_{IR}),$$

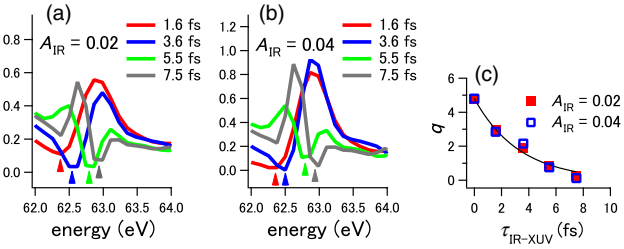

FIG. 4 (color online). (a)–(b) Sliced spectra of $S^{RES}_{3d^8}(\mathbf{k}, \tau_{IR\text{-}XUV})$ focusing on the first-order ($n = 1$) Fano sideband resonance with respect to $\tau_{IR\text{-}XUV}$ for $A_{IR} = 0.02$ and $A_{IR} = 0.04$, taken from the lower panels of Figs. 2(a) and 2(b), respectively. Arrows show $E = E^{n=1}_{RES} - q/\tau_h$. $E^{n=1}_{RES} = 62.9$ eV. (c) Asymmetry factor q of the first-order Fano sideband resonance with respect to $\tau_{IR\text{-}XUV}$.

taking $\langle 1_E^{n=0}|\mathcal{H}|1_E^{n=1}\rangle \propto e^{-\tau/\tau_h} A_{IR}(\tau - \tau_{IR\text{-}XUV})$ with an assumption of $\bar{\tau}_{IR} < \tau_h$. Similarly, we also note

$$|E^{n=1}\rangle \propto |E^{n=0}\rangle \times e^{i\omega_{IR}\tau_{IR\text{-}XUV}} A_{IR}(\omega_{IR}),$$

taking $\langle E^{n=0}|\mathcal{H}|E^{n=1}\rangle \propto A_{IR}(\tau - \tau_{IR\text{-}XUV})$. Now q is shown to be $q \approx q_0 \times e^{-\tau_{IR\text{-}XUV}/\tau_h}$ with a cancellation of the A_{IR} dependence, where q_0 is the asymmetry factor for the zeroth-order ($n = 0$) Fano resonance. In Fig. 4(c), as a matter of fact, with little dependence on A_{IR}, q shows the relaxation behavior with respect to $\tau_{IR\text{-}XUV}$ with a characteristic time of ~3.4 fs [cf. $\tau_h = 3.49$ fs at $M = 0.1$ in Fig. 1(b)]. That is, q directly traces the core-hole relaxation dynamics in the time domain. Drescher *et al.* attempted to trace the dynamics by measuring the Auger sideband area, which would be $\sim\int d\tau A_{IR}^{2\alpha}(\tau - \tau_{IR\text{-}XUV}) e^{-\tau/\tau_h}$ with α determined from the fitting procedure [1]. However, q does not incorporate any unclear fitting procedure. To our best knowledge, q is the first finding of a true time-domain core-hole clock. When there are channels of charge transfer at the surface or interface, q may also play the role of a subfemtosecond clock for charge transfer dynamics. Finally, we claim that the present approach and deduced conclusion can be generally applied to a localized system such as an atomic or molecular system or a correlated insulator.

To summarize, in a model of the attosecond pump-probe measurement of resonant photoemission of copper dichloride, we investigated the subfemtosecond quantum correlation of the two-hole states of the system. For slow core-hole relaxation (i.e., $\tau_h \gg 1/\omega_{IR}$), we find that high-order Fano sideband resonances evolve in the energy domain on the time scale of τ_h. This is confirmed by a coherent π shift of the relative phase between the photoelectron and Auger electron at each resonance, which originates from the quantum many-body correlation in the subfemtosecond time span. Finally, we also find that the asymmetry factor q of the first-order Fano sideband resonance directly traces the core-hole relaxation in the time domain without any additional fitting procedure. This is the finding of a time-domain core-hole clock.

This research was supported by the Leading Foreign Research Institute Recruitment Program through the National Research Foundation of Korea (NRF) funded by the Ministry of Education, Science and Technology (MEST) (2012K1A4A3053565).

[1] M. Drescher, M. Hentschel, R. Kienberger, M. Uiberacker, V. Yakovlev, A. Scrinzi, Th. Westerwalbesloh, U. Kleineberg, U. Heinzmann, and F. Krausz, Nature (London) **419**, 803 (2002).
[2] R. Kienberger *et al.*, Nature (London) **427**, 817 (2004).
[3] A. L. Cavalieri *et al.*, Nature (London) **449**, 1029 (2007).

[4] F. Krausz and M. Ivanov, Rev. Mod. Phys. **81**, 163 (2009) and references therein.
[5] M. Schultze *et al.*, Science **328**, 1658 (2010).
[6] J. M. Schins, P. Breger, P. Agostini, R. Constantinescu, H. Muller, G. Grillon, A. Antonetti, and A. Mysyrowicz, Phys. Rev. Lett. **73**, 2180 (1994).
[7] O. Smirnova, V. S. Yakovlev, and A. Scrinzi, Phys. Rev. Lett. **91**, 253001 (2003).
[8] J. D. Lee, Phys. Rev. B **86**, 035101 (2012).
[9] U. Fano, Phys. Rev. **124**, 1866 (1961).
[10] R. P. Madden and K. Codling, Phys. Rev. Lett. **10**, 516 (1963).
[11] C. Guillot, Y. Ballu, J. Paigné, J. Lecante, K. Jain, P. Thiry, R. Pinchaux, Y. Pétroff, and L. Falicov, Phys. Rev. Lett. **39**, 1632 (1977).
[12] G. van der Laan, C. Westra, C. Haas, and G. A. Sawatzky, Phys. Rev. B **23**, 4369 (1981).
[13] G. van der Laan, Solid State Commun. **42**, 165 (1982).
[14] S. Hüfner, *Photoelectron Spectroscopy* (Springer-Verlag, Berlin-Heidelberg, 2003).
[15] H. Wang, M. Chini, S. Chen, C.-H. Zhang, F. He, Y. Cheng, Y. Wu, U. Thumm, and Z. Chang, Phys. Rev. Lett. **105**, 143002 (2010).
[16] S. Gilbertson, M. Chini, X. Feng, S. Khan, Y. Wu, and Z. Chang, Phys. Rev. Lett. **105**, 263003 (2010).
[17] See Supplemental Material at http://link.aps.org/supplemental/10.1103/PhysRevLett.111.027401 for physical meaning of two holes "1" and "2."
[18] See Supplemental Material at http://link.aps.org/supplemental/10.1103/PhysRevLett.111.027401 for significance of M in theoretical and experimental respects.
[19] M. Kitzler, N. Milosevic, A. Scrinzi, F. Krausz, and T. Brabec, Phys. Rev. Lett. **88**, 173904 (2002).
[20] See Supplemental Material at http://link.aps.org/supplemental/10.1103/PhysRevLett.111.027401 for photon source arrangement in attosecond resonant photoemission.
[21] See Supplemental Material at http://link.aps.org/supplemental/10.1103/PhysRevLett.111.027401 for conversion of unit of laser intensity.